PCCP

Accepted Manuscript

ROYAL SOCIETY OF CHEMISTRY

www.rsc.org/pccp

ARTICLE TYPE www. rsc.org/xxxxxx | XXXXXXXX

Cross over from 3D variable range hopping to 2D weak localization conduction mechanism in disordered carbon with the extent of graphitization

Kovummal Govind Raj[1,2] **and Pattayil Alias Joy**[1,2,*]

Received Xth XXXXXXXXXX 20XX, Accepted Xth XXXXXXXXX 20XX
First published on the web Xth XXXXXXXXXX 20XX
DOI: 10.1039/b000000x

The changes in the electrical transport properties and mechanism of conduction in disordered carbon, with the extent of graphitization, are studied and discussed. With heat treatment induced graphitic ordering, the electrical properties are considerably modified, inducing a crossover from strong localization to weak localization behavior. Accordingly, the conduction mechanism is modified from 3-dimensional variable range hopping (3D VRH) model to 2-dimensional weak localization (2D WL) model. Results show that carrier-carrier and carrier-phonon interactions play major roles in developing the weak localization behavior with the extent of graphitization.

1 Introduction

Disordered carbon consists of both sp^3 and sp^2 hybridized carbon atoms distributed in different proportions.[1,2] Among these, both the sp^2 and sp^3 carbons give rise to the σ valence and σ^* conduction states separated by a large gap ($\sim$4-6 eV) and the weak π bonds arising from sp^2 carbons form the π-π^* states occupying the larger gap formed between the σ states.[1] Because of this difference, the sp^3-rich carbon systems have less density of states near the Fermi level, compared to the sp^2-rich systems. The π states formed by the sp^2 carbon atoms are sensitive towards the sp^3 to sp^2 ratio, their geometrical correlation, clustering of sp^2 carbon atoms etc.[2] Therefore, a modification in the electronic properties with clustering of the sp^2 carbon atoms is expected because of the difference in the band structure owing to the difference in the bonding characteristics and extent of spacial correlation between the sp^2 carbon sites.[3] For disordered carbons, heat treatment is known to aid structural ordering by thermally assisted clustering of sp^2 carbon atoms, along with the migration of sp^3 defects, thereby decreasing considerable strain energy associated with a randomly distributed sp^3/sp^2 structure.[4,5] For a pre-graphitic system, where chains and clusters of benzenoid networks are embedded in an sp^3 matrix, the electronic properties critically depend on the extent of graphitization and will be different from that of any other system with less number of benzenoid network or degree of clustering.[6,7]

The extent of structural ordering or graphitization in carbon structures depends on the heat treatment temperature (HTT).[8] The heat treatment driven structural ordering modifies the electrical properties in disordered carbon and enhances the conductivity, thereby developing a metallic state which can be directly observed from the changes in the temperature dependance of resistivity. The HTT driven insulator-metal (I-M) transition has been previously observed in thin films of non-graphitic disordered carbon, amorphous carbon fibers etc.[8,9] Different models have been used to describe the electrical properties in both the regimes. In the insulating side of the transition, the conduction process is governed by hopping of charge carriers between the π and π^* levels by different mechanisms. The Mott variable range hopping (VRH) and thermally assisted hopping of charge carriers have been reported as the possible mechanisms of conduction in the different disordered carbon forms.[10–12] The Mott VRH model, based on the thermally assisted hopping of charge carriers between the localized states near the Fermi level, is given by equation 1, where T_0 is the characteristic Mott temperature which depends on the electronic structure, density of states near Fermi level and localization length, ρ_0 is the pre-exponential factor and $\beta = \frac{1}{d+1}$ for d-dimensional conduction.[13,14]

$$\rho(T) = \rho_0 exp\left(\frac{T_0}{T}\right)^{\beta} \quad (1)$$

The fundamental assumption of Mott VRH theory is that the density of states near the Fermi level is constant.[13] Later Efros and Shklovskii showed that the density of states near the Fermi level may vanish, creating a gap near the Fermi level, called the Coulomb gap (CG), due to the long-range Coulomb interaction between the localized electrons.[15] The electrical

[1] *Physical and Materials Chemistry Division,* [2] *Academy of Scientific and Innovative Research, CSIR-National Chemical Laboratory, Pune 411008, India. Fax: 91 20 2590 2636; Tel: 91 20 2590 2273; E-mail: pa.joy@ncl.res.in*

transport property is then governed by equation 1, with β = 1/2 (d = 1), and this model is known as CG VRH or the Efros-Shklovskii (ES) type VRH conduction. A crossover from Mott VRH to CG VRH has been observed in different systems such as disordered carbon films,[8] boron doped carbon,[16] thin films of In_xO_y,[17] etc. Apart from VRH, thermally activated hopping due to the thermal excitation of charge carriers from localized states to the extended states of the energy band and multi-phonon tunneling due to the weak lattice carrier coupling in a delocalized π system has also been observed to be operating in disordered carbons heat treated below 800 °C and sputtered amorphous carbon films.[10–12] In less disordered carbon samples, which are close to the metallic regime, the transport properties are modified with a weak temperature dependance of resistivity and the conduction mechanism is affected by the columbic interactions in the presence of disorder,[18] 2D weak localization,[19] etc.

Another effect which modifies the conduction mechanism is the Kondo-type scattering of the conduction electrons by magnetic impurities when present in a conducting non-magnetic lattice.[20] The magnetic impurities in a non-magnetic lattice flips the complementary electron spins to different extent, thereby scattering the two complementary electron waves asymmetrically. This effect in turn destroy their phase coherence and results in a destructive interference leading to a small increase in the resistivity at low temperatures.[20] Magnetic impurity scattering has been experimentally verified in different carbon based systems like graphene with Co adatoms and defective graphene as well as in inorganic compounds like $Yb_3Os_4Ge_{13}$ and $UCo_{0.5}Sb_2$.[21–24]. The defect induced magnetic moments in He^+ irradiated graphene have been shown to couple strongly with the conduction electrons in graphene leading to a destructive interference of election waves.[22]

The modification of the hopping conduction with HTT in the insulating regime of the I-M transition has been studied in disordered carbon films,[8] and amorphous carbon fibers.[9] However, the changes in the conduction mechanism with graphitization in the metallic side of the I-M transition has not been addressed so far. In this regime, since the extent of graphitization is much higher, the conduction mechanism gets modified due to the carrier interactions in the presence of weak disorder or due to the weak magnetic moment induced by the edge state spins of isolated graphitic clusters.[25] In this paper we report the details of the changes in the conduction mechanism with the structural ordering in amorphous carbon. Structures with large disorder shows exponential increase in resistivity at low temperatures, following the Mott VRH behavior, whereas graphitic carbon shows comparatively a temperature independent resistivity curve consistent with the weak localization behavior.

2 Experimental

Disordered carbon with different extent of graphitization was prepared by pyrolysis of coconut shell, under flowing nitrogen, as described in the literature.[25] The heat treatment temperature was varied from 600 °C to 1000 °C and the samples were labeled as HTxxx, where XXX is the heat treatment temperature. Resistivity of the thin carbon pellets (∼10 mm x ∼10 mm) were measured by the Van der Pauw method[26] using a Keithley 220 constant current source and a Keithley 196 multimeter. Resistivity of HT600 was measured using a Keithley 6517A model electrometer. X-ray diffraction (XRD) studies were performed on a PANalytical X'pert pro X-ray diffractometer using Cu Kα radiation. Raman spectra were recorded on a Horiba JY labraman HR 800 micro Raman spectrometer using 633 nm He-Ne laser.

3 Results and discussion

With the increase in the heat treatment temperature, the disordered carbon structure is known to relax to an ordered graphitic structure by the migration and clustering of sp^2 bonds in a disordered sp^3 network. Previous studies on non-graphitizable carbon indicated that the conversion from sp^3 to sp^2 hybridized state takes place only at very high temperatures ($\geq$ 1300 °C).[8] However, the migration and clustering of sp^2 carbon atoms start at much lower temperatures (∼600 °C) and the extent of clustering increases as the temperature increases, which can be monitored by X-ray diffraction and Raman spectroscopy, as reported in the literature.[4,8,27,28]

The XRD patterns of the heat-treated disordered carbon (Figure 1(a)) consist of two broad peaks, at ∼23° and ∼44°, corresponding to the (002) and the (100) Bragg reflections. From the widths of these peaks, the out-of plane (L_c) and in-plane (L_a) coherence lengths, respectively, are calculated using a Scherrer-type equation.[29,30] For HT500, both (002) and (100) peaks are very broad with intensity of the latter being much smaller when compared to the other. However, with the increase in the HTT, the widths of both the peaks decrease with an increase in the relative intensity of the (002) peak, indicating the ordering of carbon phase.[25] It is observed that the in-plane (L_a) and out-of-plane (L_c) coherence lengths increase (Figure 1(b)) from 15 to 20 Å, and from 12 to 16 Å, respectively, with the increase in the heat treatment temperature from 500 to 1000 °C. The increase in the coherence lengths shows the heat treatment induced ordering of the carbon structure.

In the Raman spectra of carbon structures, the graphitic G-peak at ∼1575 cm^{-1} corresponds to the in-plane bond stretching motion of sp^2 carbon atoms and the D-peak at ∼1335 cm^{-1}, which is otherwise absent in the spectra of perfect graphite, emerges due to the breaking of the crystal symmetry, which activates certain vibrational modes.[31] The changes

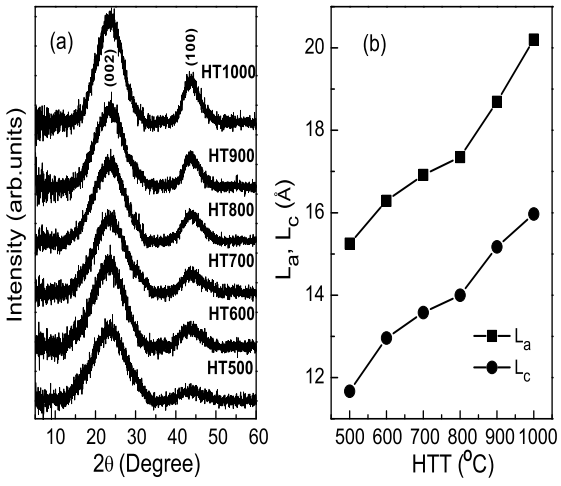

Fig. 1 (a) XRD patterns of carbon samples heat treated at different temperatures, (b) coherence lengths L_a and L_c calculated from the (100) and (002) peaks, respectively, as a function of HTT.

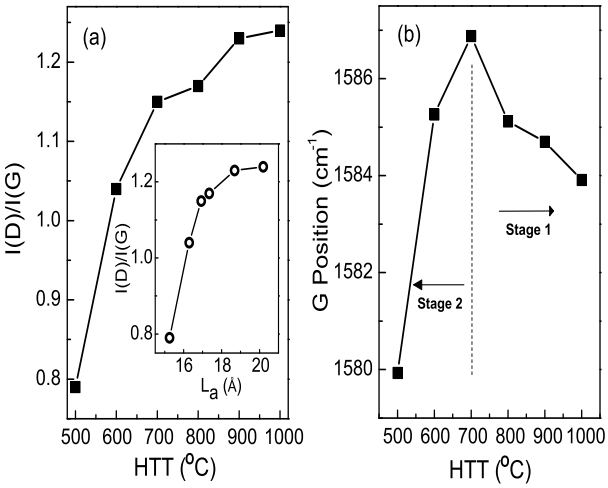

Fig. 2 (a) Changes in the I(D)/I(G) ratio with HTT and L_a (Inset), (b) variation of the G-Peak position with HTT. Solid lines are guide to the eyes.

in the vibrational density of states, with the extent of graphitization, are known to affect the D-peak to G-peak intensity ratio (I_D/I_G) as well as shifts the G-peak position in the Raman spectra and these observations have been used to track the graphitization process as described by Ferrari and Robertson using their three-stage model.[28] According to this model, the changes in the characteristics of the Raman G- and D- peaks during the ordering of a disordered carbon phase to a perfectly crystalline system, or vice-versa, can be broadly classified into three stages.[28] The boundary of stage-1 is between perfectly crystalline graphite and nanocrystalline graphite, where the I_D/I_G ratio (0–2) as well as the G-peak position (1580–1600 cm^{-1}) increases continuously due to the changes in the vibrational density of states during the conversion from monocrystalline graphite to polycrystalline graphite.[28,32] Further disorder in the nanocrystalline graphite induces a different trend for both the Raman spectral parameters. Both parameters steadily decrease due to the insertion of sp^3 defects, resulting in amorphous carbon structure ($\sim$20% sp^3) and this region is classified under stage-2. In this region, the structure consists of disordered hexagons as well as non-hexagonal rings owing to bond angle and bond-bending disorder induced due to the insertion of sp^3 defects.[28,33] With more and more sp^3 defects being inserted into the carbon structure, the extent of sp^2 clustering decreases and eventually reaches a stage where sp^2 dimers are embedded in sp^3 matrix.[28,33,34] In this region, with the increase in the sp^3 content, the G-peak position increases while the I_D/I_G ratio shows a small decrease, characterizing stage-3. In the case of the graphitization process from disordered carbon (as in the present study), the changes in the Raman spectral characteristics are expected to show a reverse trend on heat treatment, that is, transition from stage-3 to stage-1 through stage-2.

Figure 2 shows the variation of the I(D)/I(G) ratio of as well as the G-peak position, extracted from the Raman spectra, as a function of HTT. The changes in the microstructure from disordered carbon to a nanographitic structure is reflected in the I_D/I_G ratio, with a large initial increase at low HTT and a saturating behavior at higher HTT, which is characteristic of a crossover from stage-2 to stage-1, as described by Ferrari and Robertson.[28] The G-peak position also increases as the HTT increases from 500 to 700 °C, which then decreases with increasing HTT after going through a maximum for HT700. This indicates that the samples HT500 to HT700 fall under stage-2, where the I(D)/I(G) ratio and the G-peak position in the Raman spectra indicate an increase in the number of disordered hexagons with increase in HTT. On increasing the HTT above 700 °C, the shift in the G-peak position follows stage-1 behavior, which includes nanocrystalline graphite since there is considerable ordering by the formation of graphitic clusters in a disordered background owing to the ordering of hexagons and corresponding structural relaxation induced by thermal energy.[4,28] The enhancement in the values of L_a and L_c (Figure 1(b)) with HTT also occurs in a particular manner, with a larger increase from HT500 to HT600, which then becomes gradual and further increases above HT800. This shows that

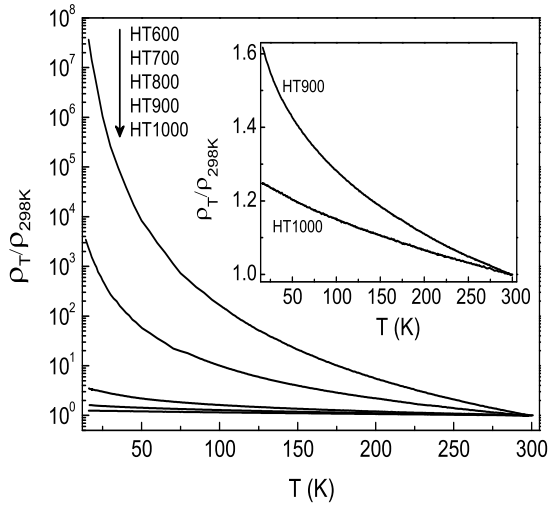

Fig. 3 Temperature variation of resistivity of different heat treated samples.

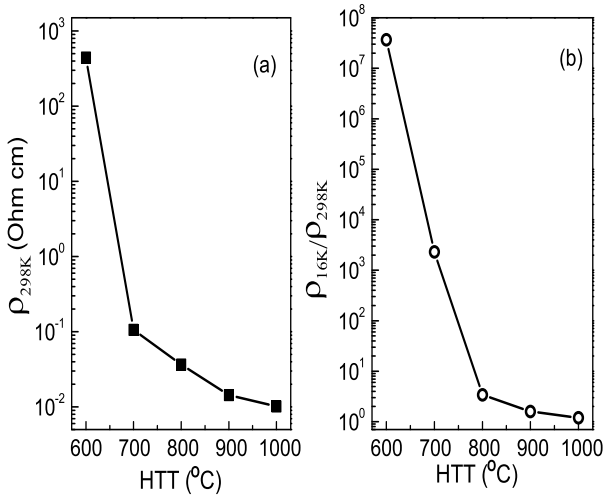

Fig. 4 Variation of (a) room temperature resistivity and (b) low-temperature to room temperature resistivity ratio with HTT. Solid lines are guide to the eyes.

the extent of graphitization is much higher in stage-1 (HT800 to HT1000) when compared to stage-2 (HT500 to HT700) and therefore supports the observed changes in the Raman spectral characteristics.

The resistivity curves of the samples heat treated from 600 to 1000 °C, as a function of temperature, are shown in Figure 3. The sample HT500 was found to be highly insulating and thus, the resistivity measurements could not be performed at low temperatures. For all the samples, the resistivity increases with decreasing temperature. The lower HTT samples (HT600 and HT700) show large increase in the resistivity on lowering the temperature, whereas for higher HTT samples (HT800, HT900, and HT1000), the resistivity curves show only a weak temperature dependance. The room temperature resistivity (ρ_{298K}) shows large changes with HTT as shown in Figure 4. HT600 has a ρ_{298K} of 450 Ohm cm, which decreases by four orders of magnitude on increasing the HTT to 700 °C. ρ_{298K} of HT800 is reduced by a factor of ten when compared to that of HT700 and on further increase in HTT, for HT900 and HT1000, the ρ_{298K} shows nearly saturating trend with much smaller decrease. The low temperature to room temperature resistivity ratio (ρ_{15K}/ρ_{298K}) also shows a similar trend, with a decrease of five orders of magnitude when HTT is increased from 600 to 700 °C and three orders of magnitude decrease from HTT 700 to 800 °C, followed by a gradual decrease.

In disordered electronic systems with large degree of disorder, the localization length, ξ, is small due to the localization of conduction electrons in a small length scale, since the benzenoid network of conduction electrons are too small with wide spatial separation.[35] The strong localization effect in disordered carbon is reflected directly in the ρ-T curve, with an exponential increase in the resistivity as temperature is decreased.[8] In heat-treated disordered carbon, the disorder depends not only on the concentration of the sp^3 defects but also on the degree of clustering of the sp^2 carbon atoms.[8] Thus, in strongly disordered systems, ξ becomes comparable to the benzenoid cluster size whereas in weakly disordered systems, ξ can be much larger, exceeding the distance that an electron travels before it encounters a scattering center or comparable to the actual size of the sample.[35,36] This decrease in the defect induced scattering of conduction electrons results in a weak temperature dependance of the ρ-T curve,[20,37] as observed for HT800, HT900 and HT1000 (Figure 3). The changes in the ρ-T behavior indicates the crossover from insulating to conducting regime. The nearly temperature independent ρ-T behavior of HT1000 shows that the sample is in the critical regime, being more towards the metallic side. The negative value of $d\rho/dT$ at higher HTT should be arising from the randomness in the nanographitic cluster size and spatial correlation. Similar changes in the room temperature resistivity as well as the low temperature to room temperature resistivity ratio, with increase in the heat treatment temperature, has been observed in amorphous carbon fibers and non-graphitic disordered carbon films prepared by PLD.[8,9] This has been interpreted as a direct consequence of the decrease in the disorder induced scattering

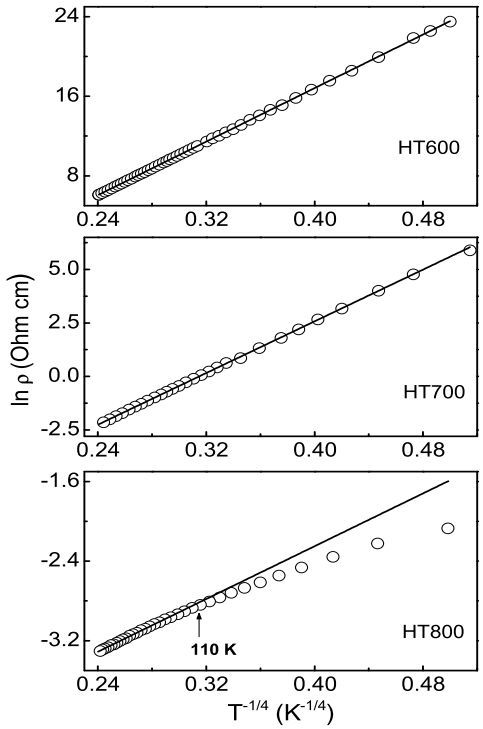

Fig. 5 Fit (solid line) to the experimental data (open circles) using the Mott 3D VRH law (equation 1). Some points in the experimental data are skipped for clarity.

of charge carriers, owing to the development of percolation pathways consisting of delocalized benzenoid networks with elevation in the structural regularity.

Carbon systems with large disorder, such as those belonging to stage-2, are expected to show variable range hopping conduction at low temperatures since the charge carriers are extremely localized due to the small cluster size.[35] The carrier transport in these materials are expected to occur through three dimensional variable range mechanism due to the randomness in the conduction pathways. Therefore the ρ-T data of the different samples are analyzed according to the Mott 3D VRH type conduction mechanism (equation 1, β = 1/4). The experimental data of HT600 and HT700 are found to fit well to the Mott 3D VRH model (Figure 5), as expected for highly disordered materials. However, for HT800, the experimental data diverges from the Mott 3D VRH law, at low temperatures (below 110 K), which is likely to be due to the modification of the conduction mechanism with structural ordering.

The value of T_0 extracted after least-squares fit to the experimental data to equation 1 (β = 1/4) for HT600, HT700 and HT800 shows a continuous decrease with increasing HTT (Table 1). The ρ_0 values are in good agreement with those ob-

Table 1 Values of T_0 and ρ_0 obtained from fitting experimental data to 3D VRH law and $N(E_F)$ values calculated by using equation 2.

Sample	ρ_0 (Ohm cm)	T_0 (K)	$N(E_F)$ ($eV^{-1}cm^{-3}$)
HT600	4.1×10^{-5}	2×10^{7}	10^{18}
HT700	7.5×10^{-4}	8×10^{5}	10^{19}
HT800	7.4×10^{-3}	2×10^{3}	10^{22}

tained for non-crystalline carbon heat-treated at similar temperatures.[11] The decrease in T_0 indicates that the mobility edge is approaching the Fermi level (E_F)with increasing HTT due to the associated structural ordering. T_0 is related to the localization length, ξ, and the density of states near the Fermi level, $N(E_F)$, through the relation shown in equation 2 and these are important parameters which indicate the extent of localization in a disordered electronic system.[38]

$$\xi = \left[\frac{k_B T_0 N(E_F)}{18}\right]^{-\frac{1}{3}} \quad (2)$$

In highly disordered carbon, where the charge carriers are extremely localized, the localization length can be taken as the effective coherence length or the graphitic cluster size calculated from the XRD data.[35] Therefore, the $N(E_F)$ values are calculated using equation 2, after substituting the L_a values calculated from XRD data for ξ. The increase in $N(E_F)$ with HTT (Table 1) is consistent with the evolution of band structure in disordered carbon by the introduction of localized states near the Fermi level due to the thermal energy assisted clustering of sp^2 carbon atoms at the expense of the strain energy.[4,39]

Due to the decrease in the structural disorder, a divergence from the 3D VRH law, with a modification of the conduction mechanism to the Coulomb gap VRH (CG VRH) law, has been observed previously in heat-treated non-graphitic disordered carbon films and boron-doped carbon.[8,16] This crossover from 3D VRH to CG VRH is due to the steep increase in the localization length with decrease in the disorder, which becomes comparable to the mean hopping length due to the elevation in the carrier density and increase in the mean free path.[16] However, in the present case, such a cross over to CG VRH or even to a Mott 2D VRH (d = 2, β = 1/3 in equation 1) mechanism was not observed for HT800 or for other higher HTT samples. The deviation from Mott 3D VRH law for HT800, along with the weak temperature dependance of resistivity observed for HT800, HT900 and HT1000, is indicative of a change in the insulating character and emergence of a semiconducting nature with the increase in the extent of graphitization. Even though the heat treatment in the temperature range 1000–1500 °C cannot induce a complete in-plane ordering, as reported,[4] this effect, previ-

ously observed in disordered carbon film, was analyzed based on the Drude model for the 2D graphene π band after considering an orientation disorder in graphene layers.[8] Similar kind of resistivity anomaly was observed in pre-graphitic carbon and this has been ascribed to the two possible factors, a small mean free path owing to the coulomb interaction in the presence of disorder or the two-dimensional weak localization (2D WL).[18–20,40] The resistivity data of HT800 and above have been analyzed based on these two models

For disordered materials, the modification in the low-temperature resistivity due to the inelastic carrier-carrier and carrier-phonon interactions is given by equation 3.

$$\sigma(T) = \sigma_0 + AT^p \quad (3)$$

The second term in equation 3 accounts for the carrier-carrier and carrier-phonon interactions.[18,37] A $T^{1/2}$ dependance of the conductivity (p = 0.5 in equation 3) is reported for disordered systems if the scattering process is dominated by carrier-carrier interactions.[18] However, if the carrier-phonon interactions dominate, the value of the exponent increases above 0.5, typically in the range 0.75 to 1.5, depending on the relative variation in the phonon wavelength and the system dimensionality determined by the extent of disorder.[37] The resistivity curve of HT800 exhibits good agreement with equation 3, as shown in Figure 6. The fitting parameters obtained are σ_0 = 0.64 Ω^{-1}cm^{-1}, A = 2.05 and p = 0.45. Since $T^{1/2}$ dependance of conductivity is characteristic of inelastic scattering by charge carrier interactions, the value of p closer to 0.5 for HT800 suggests that the carrier-carrier interaction dominates at the initial stages of graphitization.[18] As HTT is increased to 900 and 1000 °C, equation 3 remains valid for nearly in the entire high-temperature region, but a small deviation is observed at very low temperatures, with the conductivity being slightly lower than the fitted value (insets in Figure 6) and the difference increases with increasing HTT.

The 2D WL mechanism has been observed to be operative in considerably ordered pre-graphitic carbon system as well as in mechanically exfoliated graphene flakes.[19,41] 2D WL originates when the probability of elastic scattering of charge carriers by static defects is larger than the inelastic scattering due to carrier-phonon or carrier-carrier interaction.[19] In the case of graphene flakes, the scattering of charge carries can be either from inherent structural defects or graphene edges.[41] The 2D WL in graphitic clusters have been identified to produce a very small decrease in the conductivity (increase in resistivity) at low temperatures since the inelastic scattering increases as the temperature decreases, and therefore, an additional logarithmic temperature dependent term is used in equation 3, as given in equation 4.[18,40]

$$\sigma(T) = \sigma_0 + AT^p + BlnT \quad (4)$$

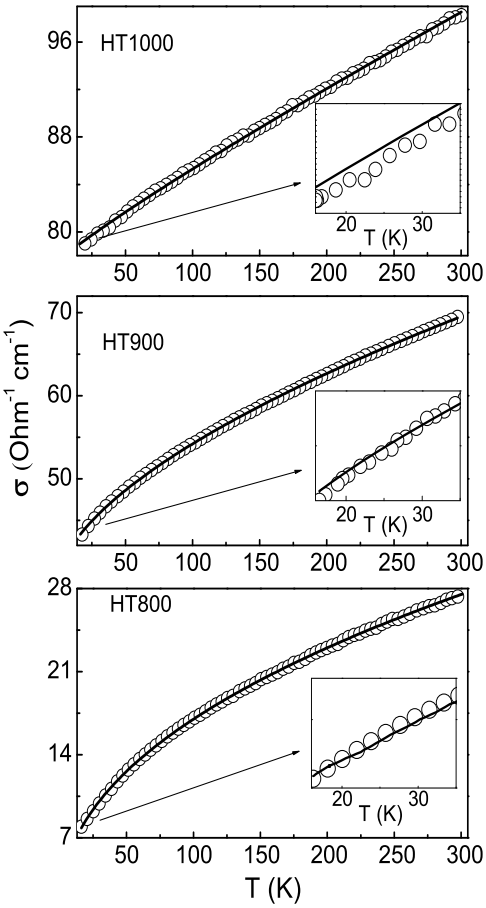

Fig. 6 Fit (solid line) to the experimental data (open circles) using equation 3. The insets show the data below 35 K. Some points in the experimental data are skipped for clarity.

On using equation 4, which includes the logarithmic correction term for weak localization interpretation, the fitted curves exactly follow the experimental data in the entire measured temperature range for both HT900 and HT1000 as shown in Figure 7 (a,b). The fitting parameters obtained for the σ-T curves of HT800, HT900 and HT1000 using equation 3 and equation 4 are listed in Table 2.

Figures 7 (c) and (d) show the temperature dependent contribution of each term in equation 4 towards the conductivity of HT900 and HT1000, respectively. The exponent term (p) of T in equation 4 for HT900 (p=0.79) and HT1000 (p=0.84) is greater than 0.5, and increases with the extent of graphitization, indicating the role of phonon mediated scattering process along with the carrier–carrier interactions.[37] For HT900, at 300 K, along with the temperature independent term σ_0 (34.40 Ω^{-1}cm^{-1}), T^p and BlnT terms contribute 22.30 Ω^{-1}cm^{-1} and

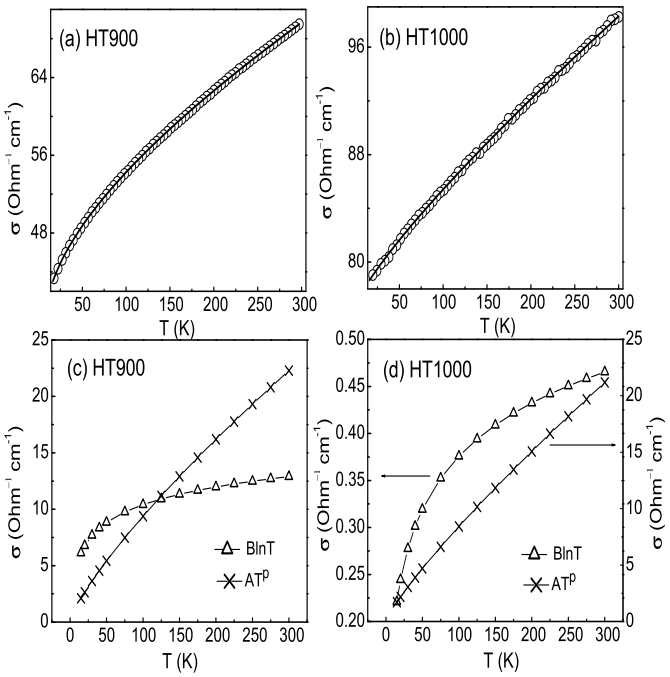

Fig. 7 Fit (solid line) to the experimental data (open circles) using equation 4 for (a) HT900 and (b) HT1000. Some points in the experimental data (a and b) are skipped for clarity. (c) and (d) show the corresponding changes in the different terms in equation 4 with temperature.

Table 2 Least squares fitted parameters using equation 3 and equation 4 (values in brackets).

Sample	$\sigma_0(\Omega^{-1}cm^{-1})$	A	p	B
HT800	0.64	2.05	0.45	-
HT900	37.80	1.04	0.60	-
	(34.40)	(0.25)	(0.79)	(2.26)
HT1000	77.50	0.12	0.90	-
	(76.60)	(0.18)	(0.84)	(0.08)

12.89 $\Omega^{-1}cm^{-1}$, respectively, towards conductivity, whereas for HT1000, T^p and BlnT terms contribute 21.18 $\Omega^{-1}cm^{-1}$ and 0.47 $\Omega^{-1}cm^{-1}$, respectively, along with the temperature independent term σ_0 (76.60 $\Omega^{-1}cm^{-1}$) (Table 2 and figures 7 (c) and (d)). For both the samples, the contribution of the exponent term decreases steadily nearly in same magnitude as the temperature is decreased and hence forms more or less a straight line with nearly same slope. However, the contributions from the 2D WL term is decreased by two order of magnitude while moving from HT900 to HT1000. This suppression of WL effect can be due to the decrease in the defect density in HT1000 when compared to that in HT900. For HT900, as the temperature is decreased below ∼120 K, the contribution from BlnT term is higher than that from T^p. This indicates an apparent higher contribution from the 2D WL term over the carrier-carrier interaction term below ∼120 K. Because of this, even though equation 4 is required to fit the experimental data in the entire temperature range, it may be noted that the experimental data deviates only to a smaller extend from equation 3 (figure 6). However, in the case of HT1000, the contribution from the BlnT term is always lower than that of the T^p term and it can also be noted that there is a considerable increase in d(BlnT)/dT below ∼ 50 K due to which the total conductivity decreases to a greater extend below this temperature when compared to the contribution at higher temperatures. Thus the 2D WL mechanism is likely to be prominent than other scattering processes, thereby inducing a small additional resistivity, particularly at very low temperatures. Hence, with graphitic ordering, depending on the extent of graphitization, the 2D WL becomes important as observed previously in pre-graphitic carbon fibers.[19]

Apart from 2D WL, magnetic impurity mediated scattering has also been observed to produce a similar decrease in the conductivity at low temperatures (equation 4).[20,22] Therefore, it is possible that this can be a possible conduction mechanism, since magnetic properties of heat treated samples showed the presence of randomly distributed intrinsically magnetic nanographitic domains of variable strength giving

rise to a spin-glass type disordered magnetic state.[25] However, the low-temperature magnetization data showed a decrease in the magnetization at 6 Tesla while moving from HT600 to HT1000. This indicates that, with heat treatment, as the cluster size increases, the magnetization decreases due to the reduction in the number of graphitic clusters as two or more clusters tend to coalesce forming larger graphitic domains.[4] Therefore, for the samples HT900 and HT1000 being considerably graphitic having lower magnetization than that of HT600, HT700 and HT800, the weak localization must be arising from the defect induced scattering at nanographitic edges rather than that arising from the scattering from magnetic impurities.

4 Conclusions

The heat-treatment induced structural ordering in disordered carbon has been shown to change the conduction mechanism with the extent of graphitization. In samples heat treated at lower temperatures ($<$ 800 °)C, there is strong localization due to the smaller graphitic cluster size and their wide spatial distribution, leading to an exponential increase in the resistivity at low temperatures showing activated hopping mechanism. On the other hand, those samples heat-treated at 900 and 1000 °C showed weak temperature dependance, showing a cross over of the conduction mechanism from 3D Mott VRH to 2D WL, due to the difference in the defect density and their spatial distribution. Thus, the extent to which different scattering mechanisms operate depends on the degree of graphitization. In the graphitic regime, the development of percolation conduction pathways, involving spatially correlated nanographitic regions, is likely to be responsible for the 2D weak localization. Magnetic impurity mediated scattering is another possible mechanism for the weak localization in the the samples heat-treated at 900 and 1000 °C. However, it is unlikely that the weak temperature dependance of resistivity of these samples originates from the magnetic impurity scattering because these samples are weakly magnetic when compared to those which followed activated hoping conduction. A high field magnetoresistance study is essential for ruling out the role of the magnetic impurity mediated scattering in the samples heat treated at higher temperatures.

Acknowledgements

KGR is grateful to the Council of Scientific and Industrial Research (CSIR), India, for a research fellowship.

References

1 C. W. Chen and J.Robertson, *J. Non-Cryst. Solids*, 1998, **227**, 602-606.
2 J. Robertson, *Prog. Solid State Chem.*, 1991, **21**, 199-333.
3 E. Staryga and G. W. Bak, *Diamond Relat. Mater.*, 2005, **14**, 23-34.
4 F. G. Emmerich, *Carbon*, 1995, **33**, 1709-1715.
5 R. Gago, M. Vinnichenko, H. U. Jager, A. Yu. Belov,I. Jimenez, N. Huang, H. Sun and M. F. Maitz, *Phys. Rev. B*, 2005, **72**, 014120(1-9).
6 M. Theye and V. Paret, *Carbon*, 2002, **40**, 1153-1166.
7 J. Robertson and E. P. O'Reilly, *Phys. Rev. B*, 1987, **35**, 2946-2957.
8 K. Takai, M. Oga, H. Sato, T. Enoki, Y. Ohki, A. Taomoto, K. Suenaga and S. Iijima, *Phys. Rev. B*, 2003, **67**, 214202(1-11).
9 A. W. P. Pung, M. S. Dresselhaus and M. Endo, *Phys. Rev. B*, 1993, **48**, 14953-14962.
10 K. Shimakawa and K. Miyake, *Phys. Rev. B*, 1989, **39**, 7578-7584.
11 F. Carmona, P. Delhaes, G. Keryer and J. P. Manceau, *Solid State Commun.*, 1974, **14**, 1183-1187.
12 K. Shimakawa and K. Miyake, *Phys. Rev. Lett.*, 1988, **61**, 994-996.
13 N. F. Mott, *Adv. Phys.*, 1967, **61**, 49-144.
14 N. F. Mott and E. A. Davis, *Electronic Process in Non-crystalline Materials*, 2nd Edition, Oxford University Press, Oxford, 1979.
15 A. L. Efros and B. I. Shklovskii, *J. Phys. C:Solid State Phys.*, 1975, **8**, L49-L51.
16 P. Vishwakarma and S. V. Subramanyam, *J. Appl. Phys.*, 2006, **100**, 113702(1-5).
17 R. Rosenbaum, *Phys. Rev. B*, 1991, **44**, 3599-3603.
18 B. L. Altshuler and A. G. Aronov, *Solid State Commun.*, 1979, **30**, 115-117.
19 V. Bayot, L. Piraux, J. P. Michenaud and J. P. Issi, *Phys Rev B*, 1989, **40**, 3514-3523.
20 G. Bergmann, *Phys Rep*, 1984, **107**, 1-58.
21 J. Ren, H. Guo, J. Pan, Y. Y. Zhang, X. Wu, H. G. Luo, S. Du, S. T. Pantelides and H. J. Gao, *Nano lett.*, 2014, **14**, 4011-4015.
22 J. H. Chen, L. Li, W. G. Cullen, E. D. Williams and M. S. Fuhrer, *Nat. Phys.*, 2011, **7**, 535-538.
23 C. L. Yang, X. Wang, X. Zhang, D. S. Wu, M. Liu, P. Zheng, J. Y. Yao, Z. Z. Li, Y. F. Yang, Y. G. Shi, J. L. Luo and N. L. Wang, *Phys. Rev. B* , 2015, **91**, 075120(1-7).
24 V. H. Tran, R. Troc, Z. Bukowski, D. Badurski, and C. Sulkowski, *Phys. Rev. B*, 2005, **71**, 094428(1-10).
25 K. G. Raj and P. A. Joy, *Solid State Commun.*, 2014, **177**,

89-94.
26 L. J. Van der Pauw, *Philips Res. Rep.*, 1958, **13**, 1-9.
27 M. Chhowalla, A. C. Ferrari, J. Robertson and G. A. J. Amaratunga, *Appl. Phys. Lett.*, **76**, 1419-1421.
28 A. C. Ferrari and J. Robertson, *Phys. Rev. B*, 2000, **61**, 14095(1-20).
29 J. Biscoe and B. E. Warren, *J. Appl. Phys.*, 1942, **13**, 364-371.
30 N. Iwashita, C. R. Park, H. Fujimoto, M. Shiraishi and M. Inagaki, *Carbon*, 2004, **42**, 701-714.
31 F. Tuinstra and J. L. Koening, *J. Chem. Phys.*, 1970, **53**, 1126-1130.
32 P. Lespade, R. Al-Jishi and M. S. Dresselhaus, *Carbon*, 1982, **20**, 427-431.
33 T. Kohler, T. Frauenheim and G. Jungnickel, *Phys. Rev. B*, 1995, **52**, 11837-11844.
34 U. Stephan, T. Frauenheim, P. Blaudeck and J. Jungnickel, *Phys. Rev. B*, 1994, **50**, 1489-1501.
35 K. Sreedhar and P. A. Joy, *Solid State Commun.*, 1996, **99**, 589-593.
36 S. Y. Hsu and J. M. Valles Jr, *Phys. Rev. Lett.*, 1995, **74**, 2331-2334.
37 P. A. Lee and T. V. Ramakrishnan, *Rev. Mod. Phys.*, 1985, **57**, 287-337.
38 Q. Guo and S. J. Poon, *Phys. Rev. B*, 1996, **54**, 12793-12797.
39 M. J. Matthews, M. S. Dresselhaus, N. Kobayashi, T. Enoki, M. Endo and K. Nishimura, *Phys. Rev. B*, 1999, **60**, 4749-4756.
40 E. P. Sajitha, V. Prasad and S. V. Subramanyam, *J. Appl. Phys.*, 2009, **105**, 073708(1-6).
41 F. V. Tikhonenko, D. W. Horsell, R. V. Gorbachev and A. K. Savchenko, *Phys. Rev. Lett.*, 2008, **100**, 056802(1-4).